

Material Properties of Si-Ge/Ge Quantum Wells

Rebecca K. Schaevitz, Jonathan E. Roth, *Member, IEEE*, Shen Ren, Onur Fidaner, *Member, IEEE*, and David A. B. Miller, *Fellow, IEEE*

Abstract—Germanium (Ge) and silicon-germanium (Si-Ge) have the potential to integrate optics with Si IC technology. The quantum-confined Stark effect, a strong electroabsorption mechanism often observed in III–V quantum wells (QWs), has been demonstrated in Si-Ge/Ge QWs, allowing optoelectronic modulators in such group IV materials. Here, based on photocurrent electroabsorption experiments on different samples and fitting of the resulting allowed and nominally forbidden transitions, we propose more accurate values for key parameters such as effective masses and band offsets that are required for device design. Tunneling resonance modeling including conduction band nonparabolicity was used to fit the results with good consistency between the experiments and the fitted transitions.

Index Terms—Germanium (Ge), optical interconnects, quantum-confined Stark effect (QCSE), silicon (Si).

I. INTRODUCTION

COMPATIBILITY with silicon (Si) IC technology has been a driving force for integrating optics on-chip, which has the potential for relieving the scaling problem currently associated with electrical interconnects [1]–[4]. Optical interconnects have many potential advantages over electrical approaches: design simplification, architectural advantages, improved timing, as well as other physical benefits such as reduced power dissipation and high densities [1], [2]. To modulate light for optical interconnects or networks, current Si-based approaches employ relatively weak effects, such as carrier-density-dependent refractive index change [5], so the resulting devices require long optical path lengths, as in long waveguides [6], or highly resonant cavities [7], to be viable. These devices can also require high drive voltages [6] or only function over a very narrow bandwidth [7] because of the weak effects employed. Stronger effects, such as the quantum-confined Stark effect (QCSE) electroabsorption [8] that can be seen in quantum-confined structures such as quantum wells (QWs), have generally only been observed in compound semiconductors, such as the III–V materials AlGaAs and GaAs [9]. While many techniques and designs

have proven successful in integrating III–V based optical devices in Si, many practical problems and concerns currently make it challenging [1]. To match the performance of III–V based optoelectronic modulators while allowing for integration into Si IC technology, a similar strong electrooptic effect is necessary in group IV materials.

In 1994, Yaguchi, *et al.*, demonstrated quantum confinement in Si-Ge/Ge heterostructures grown on germanium (Ge) substrates [10]. Early attempts at inducing the QCSE in a Si-Ge/Si material system had limited success in part because of a small conduction band offset that led to weak confinement of the exciton [11]. Recently, however, the QCSE was demonstrated in Si-Ge/Ge QWs grown on a Si substrate [12]–[14], and the first modulator devices based on the QCSE in such wells have now been demonstrated [15]–[17]. Given this success, for future device design, it is now important to refine our knowledge of key material parameters, such as effective masses and band offsets. In this paper, we address these parameters by fitting transition energies as a function of applied electric field in two different QW samples. Measuring transition energies with applied field is a particularly useful technique; a broad range of different transitions become at least partially allowed as the field is applied, hence, giving a large variety of data to provide strong constraints on the resulting fitted parameters [18].

In Section II of this paper, we will present the Si-Ge/Ge sample structures used. Specific structure fabrication techniques and experimental setups as well as experimental results will be discussed in Sections III and IV. Modeling and analysis of the experimental results will follow in Sections V and VI. Section VII summarizes and discusses future directions.

II. SAMPLE DESIGN AND BAND STRUCTURE

The basic sample design consists of a p-i-n diode with multiple QWs embedded in the intrinsic region, as shown in Fig. 1(a). The highly doped n- and p- (buffer) regions are composed of 10% Si and 90% Ge ($\text{Si}_{0.1}\text{Ge}_{0.9}$) and the nominally strain-balanced QW structure consists of pure Ge wells with $\text{Si}_{0.16}\text{Ge}_{0.84}$ barriers.

The band structures of Si and Ge, used to form the device, are sketched in Fig. 2. Since Si and Ge are both indirect bandgap materials, the global conduction band minima are not at zone center. Si's indirect gap is at the Δ valleys along the (100) crystal directions and Ge's is at the L points in the (111) directions, shown in Fig. 2(a) and (b), respectively. The composite $\text{Si}_{1-x}\text{Ge}_x$ material used in the barrier will have a Ge-like, L , indirect gap when $x > 0.85$, shown in Fig. 2(c), and a Si-like, Δ , gap otherwise [19]. To form a type-I QW and induce the QCSE, however, the confinement of the exciton must be from the direct (zone center) band edge. Ge has a relatively small direct bandgap of ~ 0.8 eV from

Manuscript received December 4, 2007; revised February 5, 2008. This work was supported in part by the Defense Advanced Research Projects Agency (DARPA)/Army Research Office (ARO) EPIC and Ultraperformance Nanophotonic Intrachip Communication (UNIC) Programs, in part by the Microelectronics Advanced Research Corporation (MARCO)/DARPA Focus Center Research Program (FCRP) Interconnect Focus Center (IFC), and in part by the National Science Foundation Graduate Research Fellowship Program (NSF GRFP).

R. K. Schaevitz, J. E. Roth, S. Ren, and D. A. B. Miller are with the Electrical Engineering Department, Stanford University, Stanford, CA 94305 USA (e-mail: rschaevitz@stanford.edu; jonroth@standfordalumni.org; renshen@stanford.edu; dabm@standford.edu).

O. Fidaner was with the Stanford University, Stanford, CA 94305 USA. He is now with Photonic Corporation, Culver City, CA 90094 USA (e-mail: ofidaner@standfordalumni.org).

Color versions of one or more of the figures in this paper are available online at <http://ieeexplore.ieee.org>.

Digital Object Identifier 10.1109/JSTQE.2008.918935

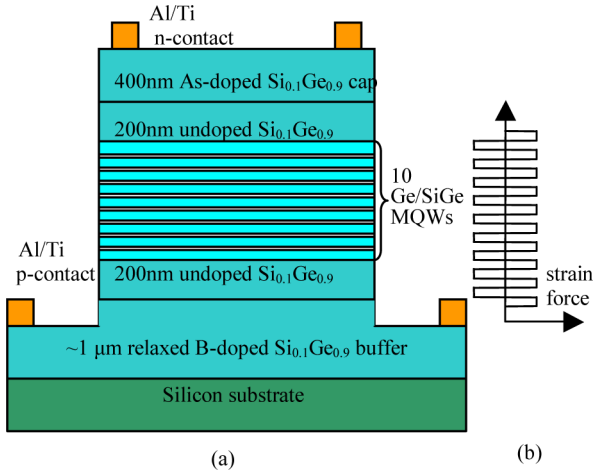


Fig. 1 (a) Mesa structure of p-i-n diode with multiple QWs in the intrinsic region. (b) Corresponding strain diagram [12].

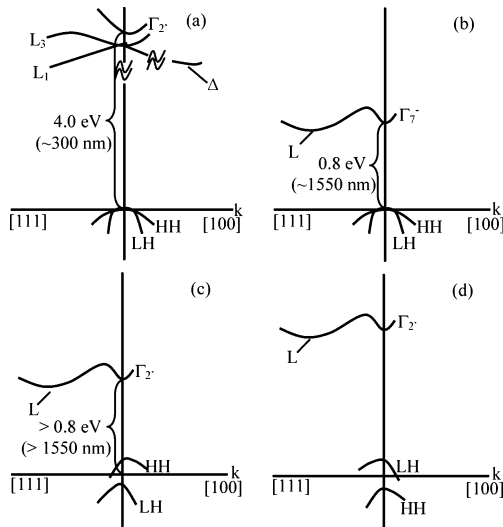


Fig. 2 Cartoon depiction of the bandstructures. (a) Ge. (b) Si. (c) Compressive strained Ge. (d) Tensile strained Ge-rich Si-Ge [12]. [100]—“z” cube edge direction, [111]—cubic space diagonal direction, Γ —“zone-center” ($k = 0$) point, L—“zone-edge” point in [111] direction, Δ —point in [100] direction with minimum energy in Si conduction band, LH—“light hole” valence band, HH—“heavy hole” valence band L_1, L_3, Γ'_2 —specific Si conduction bands.

the valence band to the Γ'_2 band [see Fig. 2(b)] [20]. This energy gap corresponds to approximately 1550 nm wavelength, which is directly in the C-band employed in many telecommunication systems. Si’s corresponding Γ'_2 bandgap [see Fig. 2(a)] is much higher, at approximately 4.0 eV [21].

When combining Si and Ge to form a QW, strain is induced due to the lattice mismatch of approximately 4.2% [22] between the pure crystals. Compressive strained Ge wells and tensile strained $\text{Si}_{1-x}\text{Ge}_x$ barriers are designed to give an overall strain-balanced QW structure with an average material composition of the surrounding $\text{Si}_{1-z}\text{Ge}_z$ regions. The basic strain diagram for the multiple QWs is shown in Fig. 1(b). The induced strain results in splitting of the heavy hole (HH) and light hole (LH) valence bands into its components as well as a change in the overall bandgap (E_g) and changes in the in-plane effec-

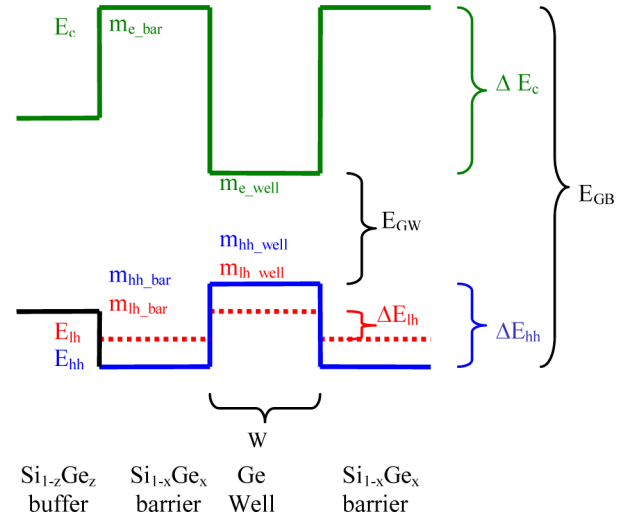


Fig. 3 Cartoon depiction of Si-Ge/Ge heterostructure (at zone center) on a Si-Ge substrate with important modeling parameters specified.

tive masses of the hole bands [23]. The compressive strain in the Ge wells causes the HH band to shift up, the LH band to shift down, and the overall bandgap to increase, as depicted in Fig. 2(c). Conversely, Fig. 2(d) shows that the tensile strain in the $\text{Si}_{0.16}\text{Ge}_{0.84}$ barriers shifts the HH and LH bands oppositely to that of the well and decreases the overall bandgap. By strain balancing, we are able to maintain stability in the structure, and hence, achieve uniform QWs. The corresponding QW band diagram on the relaxed substrate is given in Fig. 3.

III. SAMPLE FABRICATION AND EXPERIMENTAL SETUP

Two samples were used for this study that varied only in the thickness of the wells and barriers. Both samples were fabricated by Lawrence Semiconductor Research Laboratory, Inc., using reduced pressure chemical vapor deposition. The first layer grown on the (100) Si wafer is a relaxed virtual substrate, or buffer, of approximately 1 μm in thickness and composed of boron-doped $\text{Si}_{0.1}\text{Ge}_{0.9}$. This virtual substrate was grown at 500 $^\circ\text{C}$ with a constant composition of $\text{Si}_{0.1}\text{Ge}_{0.9}$ in two stages with high temperature anneals at 800 $^\circ\text{C}$ to reduce defect propagation into the active material. A thin undoped spacer layer of $\text{Si}_{0.1}\text{Ge}_{0.9}$ was followed by 10 QWs composed of pure Ge wells and $\text{Si}_{0.16}\text{Ge}_{0.84}$ barriers. For samples A and B, the thicknesses of the wells are approximately 17 and 24 nm, respectively, with the barrier thickness adjusted for strain balancing. Another thin undoped buffer layer and a final arsenic-doped layer of $\text{Si}_{0.1}\text{Ge}_{0.9}$ followed the multiple QWs. A more detailed explanation of growth can be found in [12] and [13]. Due to actual growth rates differing from expectation, the final dimensions, given in Table I, were not as originally specified by the growth recipe. Additionally, this change in thickness leads to a slightly altered strain diagram than originally intended, and we expect these samples are not exactly strain-balanced.

After epitaxial growth, the photodiode mesas were lithographically defined and samples were etched to form the mesa and deposit Ti/Al ring contacts for the n- and p-layers [see

TABLE I
QW STRUCTURE

Sample	Well Thickness (nm)	Barrier Thickness (nm)	Well Composition	Barrier Composition
A	17.8(1.5)	40.4(4)	Ge	Si _{0.16} Ge _{0.84}
B	~24.0	~50.0	Ge	Si _{0.16} Ge _{0.84}

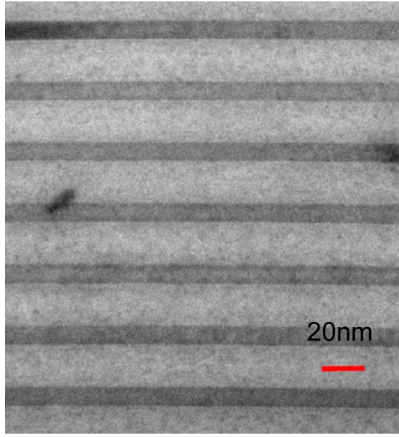


Fig. 4 TEM image along (110) of the QWs from sample A.

Fig. 1(a)]. A TEM image of our QWs for sample A is presented in Fig. 4, and the corresponding nominal well and barrier widths as deduced from such images are shown in Table I.

To gather photocurrent from these devices, the beam from one of three tunable lasers, with a combined total wavelength range of 1350–1580 nm, was focused surface-normal onto the top surface of the sample, which was antireflection coated to reduce Fabry–Perot effects. The device was reverse biased to induce an electric field ranging from, approximately, 0 to 10 V/μm. By tuning the laser and applying reverse bias, a large set of photocurrent data was obtained. Additionally, capacitance–voltage (CV) measurements were taken to better determine the electric field induced in the device for a given applied reverse bias. CV measurements also give us a better understanding of the total intrinsic region thickness and the possible unintentional doping.

IV. EXPERIMENTAL RESULTS

A. Photocurrent

Tuning over 1370–1580 nm and 0–10 V/μm leads to a significant number of observable exciton peaks. Fig. 5 gives a characteristic absorption spectrum for sample A at 25 °C. Exciton peaks are extracted from similar data and plotted as transition energy versus electric field in Fig. 6(a) and (b) for samples A and B, respectively. The spectra show a clear quadratic red shift of multiple exciton peaks for an increasing electric field, consistent with the QCSE.

B. Capacitance–Voltage

From capacitance–voltage measurements, the unintentional doping and the thickness of the intrinsic region can be deter-

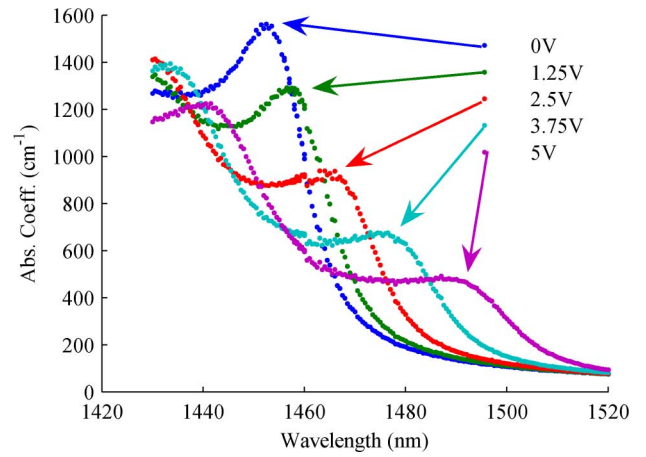


Fig. 5 Absorption spectra from photocurrent data of sample A at 25 °C.

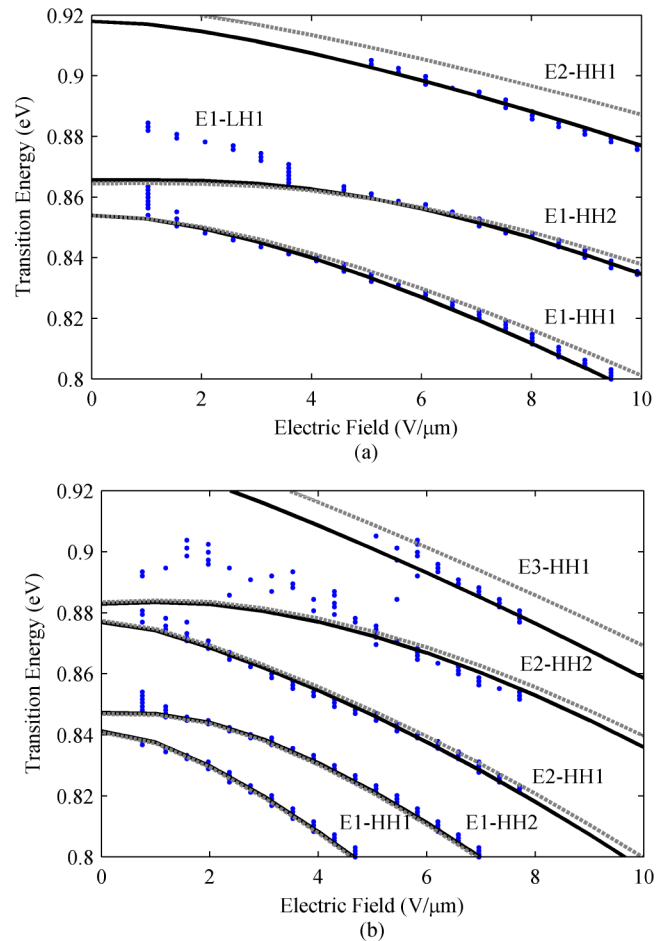


Fig. 6 Experimental (dots) versus simulation: parabolic fit (dash line), non-parabolic fit (solid line). (a) Sample A. (b) Sample B.

mined. Measurements showed an initial increase in capacitance, associated with the progressive depletion of the nominally undoped region, before the behavior resembled that of a normal p-i-n diode at higher reverse bias voltages. By modeling this behavior, we were able to estimate the unintentional doping in

the intrinsic region, at $\sim 10^{15} \text{ cm}^{-3}$, as well as the total thickness of the intrinsic region.

V. SIMULATION AND MODELING

A. Tunneling Resonance Model

Tunneling resonance transfer matrix techniques were used to calculate the quantum confinement energies in the $\text{Si}_{1-x}\text{Ge}_x/\text{Ge}$ heterostructure using boundary conditions where Ψ and $(1/m)d\Psi/dz$ are taken to be continuous (Ψ being the envelope wavefunction, and m being the effective mass). A single QW, shown in Fig. 3, was used to model all ten QWs since the large barriers prevent coupling between wells. The input parameters necessary for modeling include: mass of the HH in the well ($m_{\text{HH_well}}$) and barrier ($m_{\text{HH_bar}}$), mass of the electron in the well ($m_{\text{e_well}}$) and barrier ($m_{\text{e_bar}}$), bandgap (from the zone-center conduction band to the HH band) of the well (E_{g_well}) and barrier (E_{g_bar}), band offsets of the conduction (ΔE_C) and HH (ΔE_{HH}), as well as the width of the well (W). While LH confinement exists at least at low fields, the lack of experimental data prevents analysis comparable to that of the HH. In fact, we expect that the LH is not well confined in the presence of even moderate fields, which may explain why we see no transitions clearly associated with the LHs for most of the voltage range of these experiments. Though Fig. 6(a) does show a transition near 0.88 eV at low electric fields that we expect may be the E1–LH1 transition, we do not clearly resolve any other transitions that we can associate with any higher LH levels in either allowed or initially forbidden transitions (such as E1–LH2) in the narrow well sample [sample A in Fig. 6(a)], and we saw no clear LH transitions in the larger well sample [sample B in Fig. 6(b)]. Consequently, the LH levels will be omitted in the tunneling resonance modeling.

First, we will discuss the pertinent published experimental and theoretical values, which we used as initial values to model our heterostructure. The bulk material parameters for the electron mass, m_e , in the (100) direction presented in Table II, is presumed largely unaffected by strain. The symmetry of the conduction band around zone center results in the compressive strain having little or no effect on its effective mass in both the well and barrier. The anisotropic HH mass, in the usual k.p band structure approach, while altered substantially in the plane of the QWs or biaxially strained layers [14], [27], is presumed to remain bulk-like in the perpendicular (100) direction, at least as a first order approximation for the purposes of our model. In fitting the best value for this HH mass, we do, however, allow for significant deviation from the initial bulk values presented for the HH mass in Table II to account for both the possibility of strain mixing the hole bands, and also because of the experimental uncertainty in the prior measurements of the bulk values due to the warping of the bulk valence band. Additionally, the conduction mass of the Si Γ_2' band has not apparently been experimentally determined, leaving $m_{\text{e_bar}}$ as an unknown parameter. Theoretical values range from 0.156 [25] to 0.528 [22], resulting in a large possible variation of $m_{\text{e_bar}}$. Using linear interpolation between these Si mass values and the zone-center conduction band mass of Ge of 0.042(5) [23], the initial val-

TABLE II
SI-GE/GE EXPERIMENTAL BULK MATERIAL PARAMETERS AT 300 K

Material	$m_e(\Gamma_2)$	$m_{\text{hh}}(100)$	$m_{\text{hh}}(100)$	E_g^{direct}
Ge	0.042(5) ^a	0.284 ^b	0.044 ^b	0.797 ^c eV
Si	0.156 ^{d†}	0.537 ^e	0.153 ^e	4.00(5) ^f eV
$\text{Si}_{0.1}\text{Ge}_{0.9}$ [*]	0.0534	0.309	0.0543	1.12 eV
$\text{Si}_{0.16}\text{Ge}_{0.84}$ [*]	0.0594	0.324	0.0606	1.31 eV

^aReference [23] ^dReference [25] ^{*}Linear Interpolation
^bReference [24] ^eReference [26] [†]Theoretical Value
^cReference [20] ^fReference [21]

ues for our particular $\text{Si}_{0.16}\text{Ge}_{0.84}$ barrier material range from approximately $0.050m_0$ to $0.095m_0$.

Galdin *et al.*, performed significant theoretical work in deriving simple equations for the splitting of the HH and LH bands, ΔE_{HH} and ΔE_{LH} , of a strained $\text{Si}_{1-x}\text{Ge}_x$ on a relaxed $\text{Si}_{1-z}\text{Ge}_z$ substrate, presented in (1) and (2), for $|x-z| < 0.5$ and $z > 0.5$ [28]

$$\Delta E_{\text{HH}}(x, z) = (0.74 - 0.07z)(x - z) \quad (1)$$

$$\begin{aligned} \Delta E_{\text{LH}}(x, z) = & -0.3z + 0.289z^2 - 0.142z^3 \\ & + (0.683 - 2.58z + 3.21z^2 - 1.24z^3)x \\ & + (0.435 + 0.704z - 2.439z^2 + 1.295z^3)x^2 \\ & + \frac{(-0.354 - 3.77z + 8.79z^2 - 2.46z^3)}{(1 - 2.7z + 28.1z^2)}x^3. \end{aligned} \quad (2)$$

Assuming the barrier and well are strained relative to the substrate, on this model, the corresponding band offsets for ΔE_{HH} and ΔE_{LH} are 109 and 50.2 meV, respectively, for both samples. This low offset for the LH band, combined with its relatively low effective mass, means that the LH states will tunnel easily out of the wells with applied field, which may explain why we see little evidence of LH transitions in the presence of field and we, therefore, can conclude little about the LH behavior.

To determine the conduction band offset ΔE_C , the compressive-strain-induced increase of E_{g_well} and corresponding tensile strain induced decrease of E_{g_bar} must be quantified. Since the strain effects of the direct bandgap for both Si and Ge have not been extensively studied, a first-order assumption for the conduction band offset can be derived from a simple linear interpolation of their unaltered bandgaps, given in (3) [13]

$$\Delta E_C = (4.0 - 0.8)x - \Delta E_{\text{HH}}. \quad (3)$$

Lastly, while the TEM pictures do allow a direct measurement of well widths (see Table I), in practice, we find we need to allow some narrowing of the thicknesses compared to these numbers to get viable fits to the data. Such a correction could be justified if the interfaces between well and barrier materials are slightly graded. Because the conduction band offset in particular grows very rapidly as even small amounts of Si are incorporated, the effective well width for quantum confinement may be that corresponding to somewhere near the beginning of any such grading from the pure Ge toward the final $\text{Si}_{0.16}\text{Ge}_{0.84}$ barrier, hence, giving an effective well width somewhat narrower than the width apparent from the TEM pictures. For sample A, we

TABLE III
SI-GE/GE QW SIMULATION PARAMETERS FOR SAMPLE A

Simulation	m_{e_well}	m_{e_bar}	m_{hh_well}	m_{hh_bar}	ΔE_C (eV)	ΔE_{hh} (eV)	E_{GW} (eV)	W (nm)
1	0.041	0.0594	0.28	0.314	0.353	0.109	0.826	16.2
2	0.040	0.052-0.065	0.24	0.26-0.36	0.33-0.38	0.109	0.826	16.4
3	0.045	0.052-0.065	0.32	0.26-0.36	0.33-0.38	0.109	0.826	15.7
4	0.040	0.052-0.065	0.26-0.30	0.26-0.36	0.33-0.38	0.103	0.826	16.3
5	0.042	0.052-0.065	0.26-0.30	0.26-0.36	0.33-0.38	0.128	0.826	16.1
6	0.041	0.052-0.065	0.24	0.26-0.36	0.33-0.38	0.093	0.826	16.2

achieved fits with well thicknesses between 15.7 and 16.4 nm. For sample B, we fit the data using a well width between 22.8 and 23.8 nm.

Using the values discussed in this section and the tunneling resonance method, the best results for modeling the experimental data using simple “parabolic” effective masses are given by the broken lines in Fig. 6(a) and (b) for samples A and B, respectively. It is clear that while the first (E1–HH1) and second (E1–HH2) exciton transitions are well modeled, the higher transitions, such as E2–HH1, deviate significantly from the experimental data of sample A in Fig. 6(a). Despite significant variation in the input material parameters, the resulting simulation could not be improved if we insisted that the lowest (and practically most important) transition was to remain well fitted. Consequently, we need to look into higher order effects, such as nonparabolicity, which will be discussed in the following section.

Note, incidentally that we ignore any exciton binding energy and any shift in that energy in our modeling for the reasons discussed previously [12]: these binding energies and their shifts, being both in the range of only a few millielectron volts, are just too small to be worth including in these calculations.

B. Nonparabolicity

Materials with small direct bandgaps, such as the classic example of InSb [29], are well known to exhibit conduction band nonparabolicity. Around zone center, or zero momentum, the conduction band in zinc blende or diamond structure semiconductors is generally assumed at least as a first approximation, to be parabolic. However, as we move away from zone center to higher energies above the conduction band minimum, the parabolic assumption is no longer valid [26], [29]. At these higher energies, the bands deviate toward becoming asymptotically linear instead of parabolic, an effect that is especially pronounced in smaller bandgap materials. Since the photocurrent spectra, Fig. 6, are able to resolve higher energy electron levels, it becomes important to implement nonparabolicity in our model. A good background to nonparabolicity as well as relevant equations for implementing it in a QW is given in [30]. Specifically, the effective mass and momentum parameters were redefined using

$$m_{eNP}(\varepsilon) = m_e (1 + \alpha' \varepsilon) \quad (4)$$

$$k \approx \left[\frac{2\varepsilon m_e (1 + \alpha' \varepsilon)}{\hbar^2} \right]^{1/2} \quad (5)$$

where m_e is the electron effective mass at zone center, α' is a fitting parameter taken to be $\alpha' = 1/E_{GW}$, where E_{GW} is the direct bandgap of the well (so here $\alpha' \sim 1.25 \text{ eV}^{-1}$), and ε is the energy above the bottom of the conduction band. It is clear that (5) is simply an altered version of the standard parabolic band momentum equation ($k \approx [2\varepsilon m_e / \hbar^2]^{1/2}$), with m_{eNP} substituted for m_e . Nonparabolicity in analyzing their similar Si-Ge/Ge heterostructure was also used in [10].

The results of implementing bulk conduction band nonparabolicity for the fitting of the sample A are shown by the solid lines in Fig. 6(a). There is a dramatic improvement of the modeling of sample A for the E2–HH1 transition while maintaining excellent modeling of the first two transitions. Additionally, an excellent correspondence between simulation and data occurs when the same parameters used to model sample A, given in Table III, were then used for sample B (with a well thickness 22.8–23.8 nm), as shown by the solid lines in Fig. 6(b). While [30] derives nonparabolicity for an unstrained QW, at least in simple k.p models, strain is not expected to affect the conduction band curvature near zone center to any substantial degree. The greatly improved agreement between experiment and modeling with this nonparabolicity empirically justifies this particular simple nonparabolicity correction.

VI. DISCUSSION

While the parameters used to model samples A and B (Table III, simulation 1) result in excellent agreement with experiment, there are several other combinations of parameters that also yield similarly good results, such as those in the other simulations in Table III. Fig. 7 shows the results of the simulations using the parameters listed in Table III (broken lines) compared with the original simulations (solid line) for sample A. To understand how multiple different sets of parameters can lead to very similar simulation results, the first part of this section will briefly discuss how the specific QW parameters affect the simulation results. We will also consider some other potential effects that could distort the experimental or simulated results, thereby affecting the model.

First, we need to understand how the modeled results change as we change each of the seven parameters; specifically, we want to know in what way and with what sensitivity do the modeling results change as we change a given parameter. If there is a substantial change from a variation in one parameter, is there still some other combination of variations in other parameters that still allow us reasonably to model the data? In order to

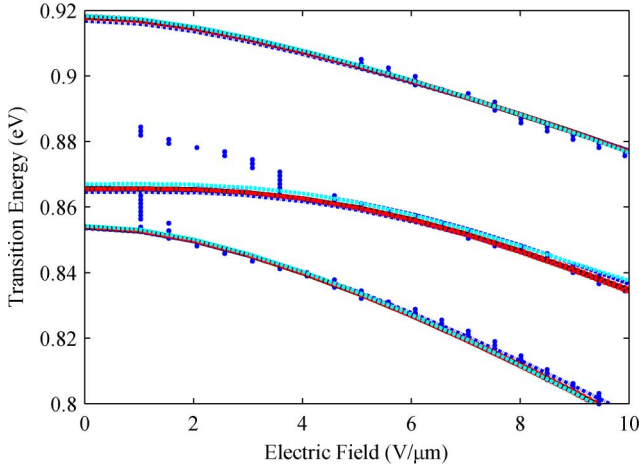


Fig. 7. Experiment versus simulation. Comparison of different parameter combinations given in Table III for sample A: simulation 1 (black solid line), simulation 2 (blue/dark grey dash line), simulation 3 (blue/dark grey dash-dot line), simulation 4 (red/medium grey dash line), simulation 5 (red/medium grey dash-dot line), and simulation 6 (cyan/light grey dash line).

answer these questions, we will focus our discussion on sample A, the results of which can easily be extrapolated to the larger well in sample B.

The well width W is one of the most important parameters in the model since it affects both the electron and HH energy levels. Changes in W affect the overall transition energy (differently for different energy levels) as well as the sensitivity to electric field. Consequently, holding all other parameters constant, W can only be altered by less than 1% if we are still to maintain reasonable fit with experiment. In contrast, $m_{\text{HH}_{\text{bar}}}$ has little impact on the transition energies or sensitivity to field and can be altered by as much as 15% from the original value. In between these two extremes are the parameters ΔE_{HH} , ΔE_C , $m_{\text{e}_{\text{well}}}$, $m_{\text{HH}_{\text{well}}}$, and $m_{\text{e}_{\text{bar}}}$, which can be altered by only 5–10% before leading to significantly different simulation results. The ranges for all parameters for different simulations have been presented in Table III and plotted in Fig. 7.

In this model, as in any, there are important tradeoffs to consider. For instance, an increase in $m_{\text{e}_{\text{well}}}$ could be offset by a decrease in $m_{\text{e}_{\text{bar}}}$ and/or an increase of ΔE_C . Similarly, an increase in $m_{\text{HH}_{\text{well}}}$ would need a corresponding increase in ΔE_{HH} to retain a good fit. Lastly, an increase in W of more than 1% could be offset by corresponding changes in the masses or band offsets of both the conduction and HH bands. While prior measurements [23] of $m_{\text{e}_{\text{well}}}$ from bulk materials constrain us to a range of 0.37–0.47 m_0 , we have little precise prior knowledge of ranges for $m_{\text{e}_{\text{bar}}}$ and ΔE_C for the QW structure. In particular, the mass of the relevant Γ'_2 Si conduction band is experimentally unknown; so, we have no prior experimental basis for a value for $m_{\text{e}_{\text{bar}}}$ even if we assume some simple linear interpolation between the Ge and Si zone center mass values. While we might assume some simple linear interpolation between the relevant bandgaps to estimate ΔE_C , again we have no real direct experimental confirmation. Fortunately, the model is relatively insensitive anyway to the values of $m_{\text{e}_{\text{bar}}}$ and ΔE_C . Consequently, the tradeoff of $m_{\text{e}_{\text{well}}}$ with

$m_{\text{e}_{\text{bar}}}$ and ΔE_C will not be considered in this discussion (or Table III), and we will mainly focus on the tradeoffs between W , $m_{\text{e}_{\text{well}}}$, $m_{\text{HH}_{\text{well}}}$, and ΔE_{HH} in the model.

As mentioned earlier, the well width W substantially impacts the transition energies as well as the sensitivity of those transition energies to field. For the E1–HH1 transition, an increase in W will result in an overall decrease in transition energy as well as greater sensitivity to field. The decrease in energy is mainly a result of the decrease in E1 whereas the sensitivity to field is more dominated by the shifts in the HH1 level. Consequently, the E1 energy decrease can be offset with a decrease in $m_{\text{e}_{\text{well}}}$ and the HH1 sensitivity with a decrease in $m_{\text{HH}_{\text{well}}}$. Additionally, it is important to look at the splitting, or overall energy difference, between levels, such as E1–E2 and HH1–HH2. Increasing W will lead to a decrease in these splittings at all electric fields. Changes in $m_{\text{e}_{\text{well}}}$ and $m_{\text{HH}_{\text{well}}}$ can also compensate for this reduction in splitting. Simulations 2 and 3 in Table III represent this tradeoff. In fact, for small changes in W , the change in overall transition energy, which is linked to the electron energy levels, is the larger effect and can be compensated only by decreasing $m_{\text{e}_{\text{well}}}$. These small changes are presented in simulations 4 and 5 in Table III.

In addition to the tradeoffs with well width W , there are also tradeoffs within the respective conduction and HH bands. Since we have already briefly discussed the tradeoff and uncertainty in ΔE_C and $m_{\text{e}_{\text{bar}}}$, in the conduction band, we will focus here on the tradeoff that exists in the HH band between $m_{\text{HH}_{\text{well}}}$ and ΔE_{HH} . An increase in $m_{\text{HH}_{\text{well}}}$ will decrease the overall energy of the corresponding transitions, especially HH2, and will slightly increase the sensitivity of the transition energy to field, though to a smaller extent than changes in W . Since an increase in ΔE_{HH} decreases the overall transition energy, and as a secondary effect, decreases the sensitivity to field for primarily HH2, the increase can offset the effect of an increase in $m_{\text{HH}_{\text{well}}}$. This correlation is presented in simulation 6 in Table III.

It is clear that excellent correspondence between data and simulation can still be preserved despite some variations of the material parameters relevant to the structure within the ranges given in the simulations in Table III. Though it is not possible to be absolutely definitive on the ranges of parameters that could give good fits given all possible tradeoffs among the seven parameters in the model, because we have considered those parameter pairs with major influences and tradeoffs, the ranges of the numbers given here are reasonable estimates of the possible ranges at least for the three parameters ΔE_{HH} , $m_{\text{e}_{\text{well}}}$, and $m_{\text{HH}_{\text{well}}}$ that are most influential in the fitting, and give indications of possible ranges for the other parameters ΔE_C , $m_{\text{e}_{\text{bar}}}$, and $m_{\text{HH}_{\text{bar}}}$ that anyway have lesser impacts on the transition energies and shifts.

In all of these simulations, incidentally, we kept a nominal HH to conduction band gap energy E_{GW} of 826 meV, which we found led to good fits. This value is approximately 26 meV higher than the unstrained Ge direct gap. Such an increase is expected because of the strain of the wells, and this particular chosen value would be explained by a compressive strain of $\sim 0.2\%$ [31].

While the simulation results that include nonparabolicity lead to excellent correspondence between experimental data and modeling, there are a few experimental sources for minor discrepancies. As can be seen in the spectra of Fig. 5, the peaks in the photocurrent spectra are not very sharp, so there is experimental uncertainty in where we should presume the centers of the peaks are. There is also underlying absorption, i.e., background absorption from other causes that underlies the direct absorption between the Ge valence and conduction bands. If the underlying absorption “slopes”, i.e., it changes as we change the photon energy, then the additive slope can change the apparent position of the exciton peak. We have taken a very simple fitting of peak position from the experimental data, without attempting to compensate for the effects of sloping background absorption from either indirect absorption or the Franz–Keldysh effect from the Si-Ge bulk layers in the structure. This does leave some uncertainty in the determination of the peak positions, but there is no simple model we can construct to take out the effects of such background absorptions.

Lastly, the slight unintentional doping in the intrinsic region leads to a slight variation in electric field across the QW region of ~ 0.5 V/ μm . This variation can lead to a broadening of the exciton peak, and possibly, a slight correction to the shift, though we have not attempted to compensate for that here.

VII. CONCLUSION

In this paper, we have experimentally measured and theoretically modeled a broad range of transitions between the electron and hole subbands in Ge QW structures with Si-Ge barriers. We have been successfully able to fit complex spectra of transitions in two different samples with one set of material parameters in a simple model. As a result, we have established a solid basis for modeling strain-balanced Si-Ge/Ge heterostructures at room temperature, and provided experimentally derived values for key parameters, especially the particularly important electron and HH effective masses in the Ge layers. One self-consistent pair of values for these parameters is, for the electron mass at the bottom of the conduction band, $m_{e_well} = 0.041$ and, for the HH mass in the (100) direction (as required for the calculation of hole confinement energies), $m_{HH_well} = 0.28$. Reasonable ranges for these and other parameters are also established. We also find that the inclusion of conduction band nonparabolicity is essential for successful modeling of transitions involving higher conduction band levels.

This research on uncoupled QWs cannot particularly give accurate values for the conduction band offset, nor for the electron or HH masses in the barrier, in large part because the energy levels in the wells are not particularly sensitive to any of these parameters; the large conduction band offsets and the large HH masses mean that there is not a very large penetration of the electron or HH wave functions into the barrier region for either the electrons or the HHs. Future work with coupled QWs may offer more precise measurements of those parameters.

ACKNOWLEDGMENT

The authors would like to thank Lawrence Semiconductor Research Laboratory, Inc., for their collaboration in growing the device structures used for this study. Additionally, the authors would like to thank Evans Analytical Group (EAG) Laboratories for their attention to detail in secondary ion mass spectrometry (SIMS) analysis.

REFERENCES

- [1] D. A. B. Miller, “Optical interconnects to silicon,” *IEEE J. Sel. Topics Quantum Electron.*, vol. 6, no. 6, pp. 1312–1317, Nov./Dec. 2000.
- [2] D. A. B. Miller, “Rationale and challenges for optical interconnects to electronic chips,” *Proc. IEEE*, vol. 88, no. 6, pp. 728–749, Jun. 2000.
- [3] D. A. B. Miller and H. M. Ozaktas, “Limit to the bit-rate capacity of electrical interconnects from the aspect ratio of the system architecture,” *J. Parallel Distrib. Comput.*, vol. 41, pp. 42–52, 1997.
- [4] H. Cho, P. Kapur, and K. C. Saraswat, “Power comparison between high-speed electrical and optical interconnects for interchip communication,” *J. Lightw. Technol.*, vol. 22, no. 9, pp. 2021–2033, Sep. 2004.
- [5] R. A. Soref, “Silicon-based optoelectronics,” *Proc. IEEE*, vol. 81, no. 12, pp. 1687–1706, Dec. 1993.
- [6] A. Liu, R. Jones, L. Liao, D. Samara Rubio, D. Rublin, O. Cohen, R. Nicolaescu, and M. Paniccia, “A high-speed silicon optical modulator based on a mental-oxide-semiconductor capacitor,” *Nature*, vol. 427, pp. 615–618, Feb. 2004.
- [7] Q. Xu, B. Schmidt, S. Pradhan, and M. Lipson, “Micrometre-scale silicon electro-optic modulator,” *Nature*, vol. 435, pp. 325–327, May 2005.
- [8] D. A. B. Miller, D. S. Chemla, T. C. Damen, A. C. Gossard, W. Wiegmann, T. H. Wood, and C. A. Burrus, “Band-edge electroabsorption in quantum well structures: The quantum-confined Stark effect,” *Phys. Rev. Lett.*, vol. 53, no. 22, pp. 2173–2177, Nov. 1984.
- [9] U. Arad, E. Redmard, M. Shamay, A. Averboukh, S. Levit, and U. Efron, “Development of a large high-performance 2-D array of GaAs-AlGaAs multiple quantum-well modulators,” *IEEE Photon. Technol. Lett.*, vol. 15, no. 11, pp. 1531–1533, Nov. 2003.
- [10] H. Yaguchi, K. Tai, K. Takemasa, K. Onabe, R. Ito, and Y. Shiraki, “Characterization of Ge/SiGe strained-barrier quantum well structures using photoreflectance spectroscopy,” *Phys. Rev. B*, vol. 49, no. 11, pp. 7394–7399, Mar. 1994.
- [11] Y. Miyake, J. Y. Kim, Y. Shiraki, and S. Fukatsu, “Absence of Stark shift in strained $\text{Si}_{1-x}\text{Ge}_x/\text{Si}$ type-I quantum wells,” *Appl. Phys. Lett.*, vol. 68, no. 15, pp. 2097–2099, Apr. 1996.
- [12] Y.-H. Kuo, Y. K. Lee, Y. Ge, S. Ren, J. E. Roth, T. I. Kamins, D. A. B. Miller, and J. S. Harris, “Quantum-confined Stark effect in Ge/SiGe quantum wells on Si for optical modulators,” *IEEE J. Sel. Topics Quantum Electron.*, vol. 12, no. 6, pp. 1503–1513, Nov./Dec. 2006.
- [13] Y.-H. Kuo, Y. K. Lee, Y. Ge, S. Ren, J. E. Roth, T. I. Kamins, D. A. B. Miller, and J. S. Harris, “Strong quantum-confined Stark effect in germanium quantum-well structures on silicon,” *Nature*, vol. 437, pp. 1334–1336, Oct. 2005.
- [14] S. Tsujino, H. Sigg, G. Mussler, D. Chrastina, and H. von Känel, “Photocurrent and transmission spectroscopy of direct-gap interband transitions in Ge/SiGe quantum wells,” *Appl. Phys. Lett.*, vol. 89, no. 26, pp. 1–262119-3, Dec. 2006.
- [15] J. E. Roth, O. Fidaner, R. K. Schaevitz, Y.-H. Kuo, T. I. Kamins, J. S. Harris, and D. A. B. Miller, “Optical modulator on silicon employing germanium quantum wells,” *Opt. Exp.*, vol. 15, no. 9, pp. 5851–5859, Apr. 2007.
- [16] J. E. Roth, O. Fidaner, E. E. Englund, R. K. Schaevitz, Y.-H. Kuo, N. C. Helman, T. I. Kamins, J. S. Harris, and D. A. B. Miller, “C-band side-entry Ge quantum well electroabsorption modulator on SOI operating at 1 volt swing,” *Electron. Lett.*, vol. 44, no. 1, pp. 49–50, Jan. 2008.
- [17] O. Fidaner, A. K. Okyay, J. E. Roth, R. K. Schaevitz, Y.-H. Kuo, K. C. Saraswat, J. S. Harris, and D. A. B. Miller, “Ge-SiGe quantum-well waveguide photodetectors on silicon for the near-infrared,” *IEEE Photon. Techn. Lett.*, vol. 19, no. 17–20, pp. 1631–1633, Sep./Oct. 2007.
- [18] K. Yamanaka, T. Fukunaga, N. Tsukada, K. L. I. Kobayashi, and M. Ishii, “Photocurrent spectroscopy in GaAs/AlGaAs multiple quantum wells under a high electric field perpendicular to the heterointerface,” *Appl. Phys. Lett.*, vol. 48, no. 13, pp. 840–842, Mar. 1986.

- [19] R. Braunstein, A. R. Moore, and F. Herman, "Intrinsic optical absorption in germanium-silicon alloys," *Phys. Rev.*, vol. 109, no. 3, pp. 695–710, Feb. 1958.
- [20] W. C. Dash and R. Newman, "Intrinsic optical absorption in single-crystal germanium and silicon at 77 K and 300 K," *Phys. Rev.*, vol. 99, no. 4, pp. 1151–1155, Aug. 1955.
- [21] D. E. Aspnes and A. A. Studna, "Direct observation of the E_0 and $E_0 + \Delta_0$ transitions in silicon," *Solid State Commun.*, vol. 11, pp. 1375–1378, 1972.
- [22] C. Tserbak, H. M. Polatoglou, and G. Theodorou, "Unified approach to the electronic structure of strained Si/Ge superlattices," *Phys. Rev. B*, vol. 47, no. 12, pp. 7104–7124, Mar. 1993.
- [23] S. H. Groves, C. R. Pidgeon, and J. Feinleib, "Infrared magnetoelectroreflectance in Ge, GaSb, and InSb," *Phys. Rev. Lett.*, vol. 17, no. 12, pp. 643–646, Sep. 1966.
- [24] R. N. Dexter, H. J. Zeiger, and B. Lax, "Cyclotron resonance experiments in silicon and germanium," *Phys. Rev.*, vol. 104, no. 3, pp. 637–644, Nov. 1956.
- [25] M. Cardona and F. H. Pollak, "Energy-band structure of germanium and silicon: The kp method," *Phys. Rev.*, vol. 142, no. 2, pp. 530–543, Feb. 1966.
- [26] H. D. Barber, "Effective mass and intrinsic concentration in silicon," *Solid-State Electron.*, vol. 10, no. 11, pp. 1039–1051, 1967.
- [27] C. M. Engelhardt, D. Tobben, M. Aschauer, F. Schaffler, G. Abstreiter, and E. Gornik, "High mobility 2-D hole gases in strained Ge channels on Si substrates studied by magnetotransport and cyclotron resonance," *Solid-State Electron.*, vol. 37, no. 4–6, pp. 949–952, 1994.
- [28] S. Galdin, P. Dollfus, V. Aubry Fortuna, P. Hesto, and H. J. Osten, "Band offset predictions for strained group IV alloys: $\text{Si}_{1-x-y}\text{Ge}_x\text{C}_y$ on Si(001) and $\text{Si}_{1-x}\text{Ge}_x$ on $\text{Si}_{1-z}\text{Ge}_z$ (001)," *Semicond. Sci. Technol.*, vol. 15, no. 6, pp. 565–572, Jun. 2000.
- [29] E. O. Kane, "Band structure of indium antimonide," *J. Phys. Chem. Solids*, vol. 1, pp. 249–261, 1957.
- [30] U. Ekenberg, "Nonparabolicity effects in a quantum well: Sublevel shift, parallel mass, and Landau levels," *Phys. Rev. B*, vol. 40, no. 11, pp. 7714–7726, Oct. 1989.
- [31] M. M. Rieger and P. Vogl, "Electronic-band parameters in strained $\text{Si}_{1-x}\text{Ge}_x$ alloys on $\text{Si}_{1-y}\text{Ge}_y$ substrates," *Phys. Rev. B*, vol. 48, no. 19, pp. 14276–14287, Nov. 1993.



Rebecca K. Schaevitz received the B.Sc. degree in electrical engineering in 2005 from Tufts University, Boston, MA, and the M.S. degree in electrical engineering in 2008 from Stanford University, Stanford, CA, where she is currently working toward the Ph.D. degree.

Her current research interests include physical properties of the Si-Ge/Ge heterostructure in order to engineer devices for silicon IC compatible optical interconnects.

Ms. Schaevitz is a Student Member of the Optical Society of America (OSA). She was recently nominated for the Best Student Paper Award at OSA's Frontiers in Optics conference, San Jose, CA, in 2007.

Jonathan E. Roth (M'07) received the B.Sc. degree in biomedical engineering from Case Western Reserve University, Cleveland, OH, in 2000, and the Ph.D. degree in electrical engineering from Stanford University, Stanford, CA, in 2007.

From 2000 to 2001, he was a Fulbright Scholar at Lund Institute of Technology, Lund, Sweden, where he was engaged in research on tissue optics and photodynamic therapy. He is currently with the Electrical Engineering Department, Stanford University.



Shen Ren received the B.Sc. degree in electrical engineering in 2004 from Peking University, Beijing, China, and the M.Sc. degree in electrical engineering in 2006 from Stanford University, Stanford, CA, where he is currently working toward the Ph.D. degree in electrical engineering.

His current research interests include quantum-confined silicon germanium structures and devices for optical interconnect applications.



Onur Fidaner (S'00–M'07) received the B.Sc. degree in electrical and electronics engineering from the Middle East Technical University (METU), Ankara, Turkey, in 2001, and the M.Sc. and Ph.D. degrees in electrical engineering from Stanford University, Stanford, CA, in 2003 and 2007, respectively.

He was a Lucent Technologies Stanford Graduate Fellowship Student at Stanford University. He was engaged in research on optical interconnects on silicon that employ the quantum-confined Stark effect (QCSE) in Ge/Si-Ge quantum well waveguide

electroabsorption modulators and detectors. He is currently with Photonic Corporation, Culver City, CA.

Mr. Fidaner was the recipient of the Student Presentation Award at Optical Society of America's (OSA) Frontiers in Optics Conference in 2007 for demonstrations of the first optical link on silicon that employs the QCSE.



David A. B. Miller (M'84–SM'89–F'95) received the B.Sc. degree in physics from St. Andrews University, in 1976, St. Andrews, U.K., and the Ph.D. degree in physics from Heriot-Watt University, Edinburgh, U.K., in 1979.

From 1981 to 1996, he was with Bell Laboratories, where, since 1987, he had been the Department Head, and later, the Advanced Photonics Research Department. From 1997 to 2006, he was the Director of the Ginzton Laboratory, Stanford. He is currently the W. M. Keck Professor of Electrical Engineering

at Stanford University, Stanford, CA, where he is the Director of the Solid State and Photonics Laboratory and the Co-Director of the Stanford Photonics Research Center. He holds honorary degrees from the Vrije Universiteit Brussel and Heriot-Watt University. His current research interests include nanophotonic and quantum-confined optoelectronic physics and devices, and fundamentals and applications of optics in information sensing, switching, and processing. He is the author or coauthor more than 200 published scientific papers, delivered talks at more than 100 conferences, and holds 62 patents.

Dr. Miller was a Board Member of the Optical Society of America (OSA) and the IEEE Lasers and Electro-Optics Society (LEOS), and in various other society and conference committees. He was the President of the IEEE Lasers and Electro-Optics Society in 1995. He has also served on the boards of various photonics companies. He is the recipient of the Adolph Lomb Medal and the R. W. Wood Prize from the OSA, the International Prize in Optics from the International Commission for Optics, and the IEEE Third Millennium Medal. He is a Fellow of the Royal Societies of London and Edinburgh, the OSA, and the American Physical Society (APS).